



**Abstract**

The upper-level jet stream impacts surface-level trace gas variability, yet the cause of this relationship remains unclear. We investigate the mechanism(s) responsible for the relationship using idealized tracers with different source regions within a chemical transport model. All tracers' daily variabilities are correlated with the meridional position of the jet stream in the mid-latitudes, but tracers emitted south (north) of the jet increase (decrease) in the mid-latitudes when the jet is poleward-shifted. The jet stream regulates the near-surface meridional wind, and this coupling together with the meridional tracer gradient robustly predicts where the jet stream and tracers are in and out of phase. Our study elucidates a major driver of trace gas variability and links it to the location of the jet stream and emissions. These results are useful for understanding changes in trace gas variability if the jet stream's position or major emission source regions change in the future.

**Plain Language Summary**

Previous studies have shown a connection between greenhouse gases or air pollutants and the jet stream, a narrow band of strong winds aloft that encircle the mid-latitudes. The mechanisms that link the jet stream to changes in greenhouse gases and air pollutants at earth's surface and how is connected to the source regions of emissions are not well understood. To address this, we use computer models of the atmosphere that include "tracers," artificial particles that track fluid motion within the atmosphere. Tracers are emitted from different latitudes in the Northern Hemisphere, ranging from the equator to the pole. All tracers are impacted by the position of the jet stream, but whether a particular tracer increases or decreases when the jet is in a poleward position is a strong function of where it was emitted. We show that the jet stream affects variations in the north-south wind at the surface, and changes in this wind lead to the advection of air with higher or lower tracer concentrations, depending on the latitudinal tracer gradient. Our findings may help interpret other atmospheric models that simulate pollution and greenhouse gases and the impacts of climate change on these species.

**1 Introduction and Motivation**

Concentrations of near-surface air pollutants and greenhouse gases exhibit large day-to-day variations, driven by a combination of variations in emissions, chemistry, and transport. Understanding the cause of this variability is paramount for interpreting measurements and trends in pollutants (e.g., Cooper et al., 2014; Dawson et al., 2014; Kerr et al., 2019) and greenhouse gases (e.g., Keppel-Aleks et al., 2011; Miller et al., 2013, 2015; Randazzo et al., 2020).

Several studies have highlighted the importance of transport in explaining the daily variability of near-surface composition. For example, daily variations of ozone ( $O_3$ ) have been linked to transport-related phenomena such as horizontal and vertical advection and frontal systems (Jacob et al., 1993; Kerr et al., 2019; Porter & Heald, 2019; Kerr et al., 2020), while Keppel-Aleks et al. (2011) and Torres et al. (2019) have shown that the variability of carbon dioxide ( $CO_2$ ) attributed to the prevailing synoptic- and mesoscale weather is of similar magnitude to the variability from local diurnal fluxes. Moreover, variations in the meridional, or north-south, position of the upper-level jet stream and its effect on transient atmospheric eddies and frontal zones have been linked to variability in near-surface particulate matter (Ordóñez et al., 2019),  $CO_2$  (Randazzo et al., 2020; Pal et al., 2020), methane (Guha et al., 2018), and  $O_3$  (Barnes & Fiore, 2013; Shen et al., 2015; Kerr et al., 2020).

A recent study by Kerr et al. (2020) provided further support for a link between variability in the upper-level jet and surface-level  $O_3$  but also showed substantial spa-

65 tial variations in the relationship. They showed that the daily variability in surface-level  
66 O<sub>3</sub> during boreal summer (JJA) is significantly correlated with the meridional position  
67 of the jet across the Northern Hemisphere mid-latitudes, but the sign of the relationship  
68 differed between land and ocean (with O<sub>3</sub> increasing over land but decreasing over the  
69 oceans when the jet is in a poleward position). Furthermore, the jet-O<sub>3</sub> relationship is  
70 weak or non-existent at high and low latitudes.

71 The findings from the aforementioned studies raise several important questions: What  
72 mechanisms connect flow aloft to near-surface composition and variability? Why does  
73 the jet-O<sub>3</sub> relationship vary with latitude and between land and ocean? How do species'  
74 lifetimes and source regions affect the relationship? The last question is important when  
75 considering the jet's role in the variability of greenhouse gases and surface-level partic-  
76 ular matter whose lifetimes and source regions differ. Increases in anthropogenic green-  
77 house gas emissions will likely shift the mean jet latitude poleward and modulate jet speed  
78 later in the twenty-first century (Barnes & Polvani, 2013). These projected changes war-  
79 rant an improved understanding of how flow aloft impacts near-surface composition, which  
80 could improve our projections of how future pollutant distributions could change.

81 We address these questions by performing chemical transport model (CTM) sim-  
82 ulations of a suite of idealized tracers with differing source regions. The simulations en-  
83 able us to examine how the Northern Hemisphere tracer-jet relationships vary with source  
84 region and under what condition(s) there are land-ocean or seasonal variations. Ideal-  
85 ized tracers can aid in understanding and interpreting the impact of the jet stream on  
86 near-surface composition while avoiding the complex interplay of non-linear gas- and particle-  
87 phase chemistry and temporally- and spatially-varying precursor emissions (e.g. Orbe  
88 et al., 2016).

89 In Section 2, we describe the CTM simulations, reanalysis, and methodology used  
90 in this study. We document the relationship of the tracers with the jet in Section 3.1 and  
91 the impact of the jet on near-surface meridional wind in Section 3.2. We find simple bal-  
92 ances that relate the connection of the jet stream with near-surface meridional wind to  
93 the meridional tracer gradient give a satisfying physical explanation to differences in the  
94 sign of the tracer-jet relationships (Sections 3.2-4).

## 95 2 Data and Methodology

96 We use the GEOS-Chem CTM (version 12.0.2) to perform our tracer simulations  
97 (Bey et al., 2001; The International GEOS-Chem User Community, 2018, October 10).  
98 GEOS-Chem is driven by assimilated meteorology from the Modern Era-Retrospective  
99 Analysis for Research and Analysis, Version 2 (MERRA-2). Three-dimensional MERRA-  
100 2 fields are input to the CTM every three hours, while surface quantities and mixing depths  
101 are provided every hour. Specifically, our configuration of GEOS-Chem follows a pas-  
102 sive simulation described in Liu et al. (2001). We perform this simulation at a resolu-  
103 tion of 2° latitude x 2.5° longitude with 72 vertical levels (~ 15 hPa spacing below 800  
104 hPa) for 2007 – 2010, and we discard the first year (2007) for spin up.

105 Previous studies have demonstrated the accuracy of transport in GEOS-Chem and  
106 the assimilated meteorological product, MERRA-2, driving the CTM. Bosilovich et al.  
107 (2015) showed that magnitude of MERRA-2 zonal and meridional wind fields as well as  
108 the location of wind maxima are well-constrained by observations and other reanalyses.  
109 GEOS-Chem yields realistic mixing ratios and seasonal and latitudinal variations of other  
110 tracers such as lead and beryllium with no significant global bias (Liu et al., 2001). How-  
111 ever, Yu et al. (2018) recently pointed out that the use of offline CTMs, such as GEOS-  
112 Chem, together with an archived assimilated meteorological product can lead to verti-  
113 cal transport errors due, in part, to loss of transient advection (resolved convection). While  
114 potential biases and errors are important to keep in mind, the extensive body of liter-

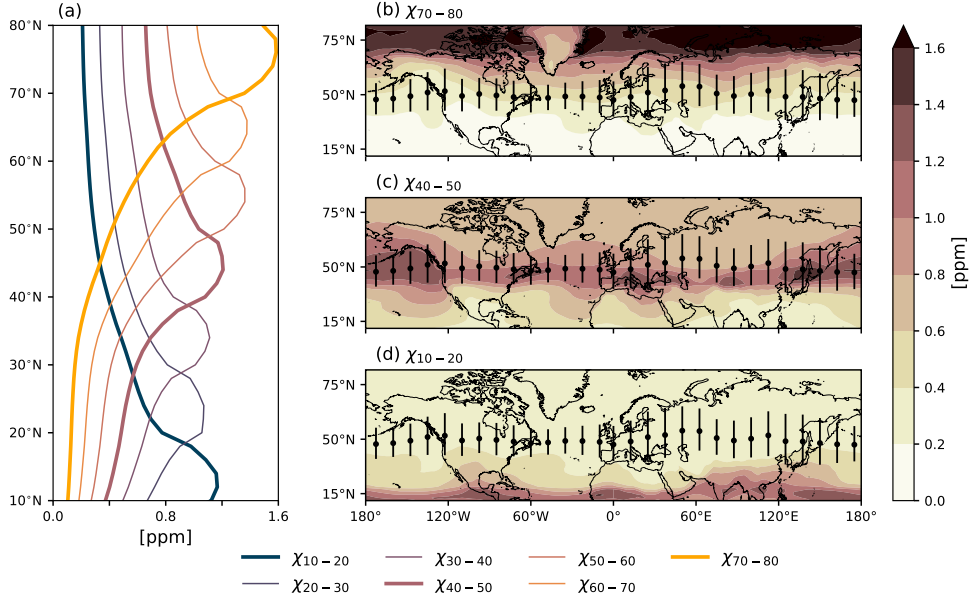


**Figure 1.** (a) Zonally-averaged tracer mixing ratios in JJA. (b) JJA-averaged mixing ratios of (b)  $\chi_{70-80}$ , (c)  $\chi_{40-50}$ , and (d)  $\chi_{10-20}$ . Scatter points and vertical bars in (b)-(d) represent the mean position and variability of the jet stream in JJA, respectively. Note that the thicker lines in (a) correspond to the tracers featured in (b)-(d).

115 ature on the reliability of GEOS-Chem supports its suitability as the framework to ad-  
 116 dress our research questions.

117 Within GEOS-Chem, we implement a suite of nine passive tracers that differ only  
 118 in their source regions, which are prescribed as constant flux boundary conditions (i.e.,  
 119 emissions) in zonally-symmetric  $10^\circ$  latitudinal bands. Tracers are herein denoted  $\chi_{\phi_1-\phi_2}$ ,  
 120 where  $\phi_1$  is the latitude corresponding to the southern boundary of the source region and  
 121  $\phi_2$  is the northern boundary. All tracers decay uniformly at a loss rate of  $\tau = 50 \text{ days}^{-1}$ .  
 122 Tracers with the same loss have been used in prior studies (e.g., Shindell et al., 2008; Orbe  
 123 et al., 2017, 2018; Yang et al., 2019). Although not the primary focus of our analysis,  
 124 we also explore how the lifetime of tracers impacts their relationship with the jet by sim-  
 125 ulating  $\chi_{40-50}$  with loss rates of  $\tau = 5, 25, 100$  and  $150 \text{ days}^{-1}$ . Unless indicated, all  
 126 analyses use daily mean near-surface (1000 – 800 hPa) tracer mixing ratios.

127 In addition to driving the GEOS-Chem simulations, we use MERRA-2 to charac-  
 128 terize the meteorology responsible for tracer variability (McCarty et al., 2016; Gelaro  
 129 et al., 2017). MERRA-2 is output on a global  $0.5^\circ \times 0.625^\circ$  grid with 72 vertical levels.  
 130 Specifically, we obtain 3-hourly 1000–800 hPa meridional wind ( $V$ ) and 500 hPa zonal  
 131 wind ( $U$ ) from MERRA-2 and average these data to daily mean values, consistent with  
 132 our treatment of tracers from GEOS-Chem. The horizontal resolution differs between  
 133 GEOS-Chem and MERRA-2, and we degrade the resolution of MERRA-2 to match that  
 134 of GEOS-Chem using xESMF, a universal regridding for geospatial data (Zhuang et al.,  
 135 2020).

136 We locate the latitudinal position of the jet stream ( $\phi_{jet}$ ) daily at each longitude  
 137 by finding the latitude (restricted to  $20-70^\circ\text{N}$ ) of maximum 500 hPa  $U$ . A simple convolution-  
 138 based smoothing is applied in longitudinal space to address potential longitudinal dis-

139 continuities in the jet’s position (i.e., “jumps” in the latitude of the jet) using a box-shaped  
 140 function with a width of  $\sim 10^\circ$  longitude (Barnes & Fiore, 2013; Kerr et al., 2020).

141 The temporal correlation between  $\phi_{jet}$  and near-surface tracer mixing ratios or  $V$   
 142 is quantified with the Pearson product-moment correlation coefficient, indicated by  $r(X, Y)$ ,  
 143 where  $X$  and  $Y$  are the time series of interest. We assess the significance of the corre-  
 144 lation coefficient using the non-parametric moving block bootstrapping method, which  
 145 preserves much of the temporal correlation in the time series and makes no *a priori* as-  
 146 sumptions about the time series’ distributions. In essence, time series  $X$  and  $Y$  are ran-  
 147 domly reordered by sampling continuous blocks of data with length = 10 days, and  $r(X, Y)$   
 148 is thereafter recalculated. We conduct 10000 realizations of this reordering, and signif-  
 149 icance is determined with a two-tailed percentile confidence interval method at the 0.05  
 150 significance level (Wilks, 1997; Mudelsee, 2003; Wilks, 2011).

151 We also generate composites of tracer mixing ratios and  $V$  on days when the jet  
 152 stream is poleward (PW) and equatorward (EW). The PW (EW) composite is defined  
 153 locally (i.e., at each longitude) as the average value of the field of interest for days where  
 154  $\phi_{jet}$  exceeds (is less than) the 70th (30th) percentile. We define a “positive” relation-  
 155 ship to mean that the PW (EW) movement of the jet is associated with increased (de-  
 156 creased) mixing ratios or  $V$ . The opposite is true for a “negative” tracer-jet relationship.

### 157 3 Results

#### 158 3.1 Relationship between the jet stream and tracers

159 Before we examine the tracers’ relationship with  $\phi_{jet}$  we briefly discuss the mean  
 160 tracer distributions and their daily variability. Zonally-averaged tracer mixing ratios peak  
 161 within their source regions and diminish to roughly half of their maximum value  $\pm 5^\circ$  out-  
 162 side their source regions (Figure 1a). Tracers with source regions at latitudes ( $\phi$ ) north  
 163 of  $60^\circ\text{N}$  have higher mixing ratios within their source regions compared with tracers emit-  
 164 ted at lower latitudes (Figure 1a), supporting an isolated Arctic lower troposphere and  
 165 the “polar dome” as a barrier to transport (Law & Stohl, 2007).

166 Despite zonally-symmetric emissions, there are zonal variations in tracer mixing  
 167 ratios (Figure 1b-d). The latitudinal range with high tracer mixing ratios ( $> 0.8$  ppm)  
 168 is larger over the ocean basins for tracers with high and mid-latitude sources (e.g.,  $\chi_{70-80}$ ,  
 169  $\chi_{40-50}$ ; Figure 1b-c). These ocean regions coincide with the Atlantic and Pacific storm  
 170 tracks. High mixing ratios of tracers with source regions in the tropics (e.g.,  $\chi_{10-20}$ ) are  
 171 more diffuse over land and more restricted over the tropical ocean (Figure 1d).

172 Spatial variations in the tracers’ daily variability (as measured by the standard de-  
 173 viation) are similar to spatial variations in their mean distribution, with highest vari-  
 174 ability near the tracer source region and decreasing to the north and south (not shown).  
 175 Furthermore the ratio of each tracer’s standard deviation to its mean is  $\sim 50\%$  near the  
 176 source region and diminishes to  $\sim 20\%$  well outside the source region (not shown).

177 To assess the impact of the meridional movement of the jet on daily tracer vari-  
 178 ability, we examine composites of tracer mixing ratios when the jet is PW and EW (see  
 179 Section 2). As is shown in Figure 2, there is a significant tracer-jet relationship for all  
 180 tracers during JJA and DJF within the mid-latitudinal range over which the jet traverses.  
 181 However, the sign of the relationship hinges on the meridional gradients of the tracers  
 182 ( $\partial\chi/\partial\phi$ ). Tracers with source regions at low latitudes ( $\phi < 40^\circ\text{N}$ ) have a negative gra-  
 183 dient ( $\partial\chi/\partial\phi < 0$ ) within the latitudinal range of the jet and increase in the mid-latitudes  
 184 when the jet is PW (Figure 2a-b). Tracers emitted around the latitude of the jet ( $40^\circ <$   
 185  $\phi < 60^\circ\text{N}$ ) have a spatially-varied gradient and relationship with the jet in the mid-  
 186 latitudes. In particular, we note the land-ocean differences in the JJA  $\chi_{40-50}$ -jet rela-  
 187 tionship (Figure 2c). Tracers with source regions at high latitudes ( $\phi > 60^\circ\text{N}$ ) are char-

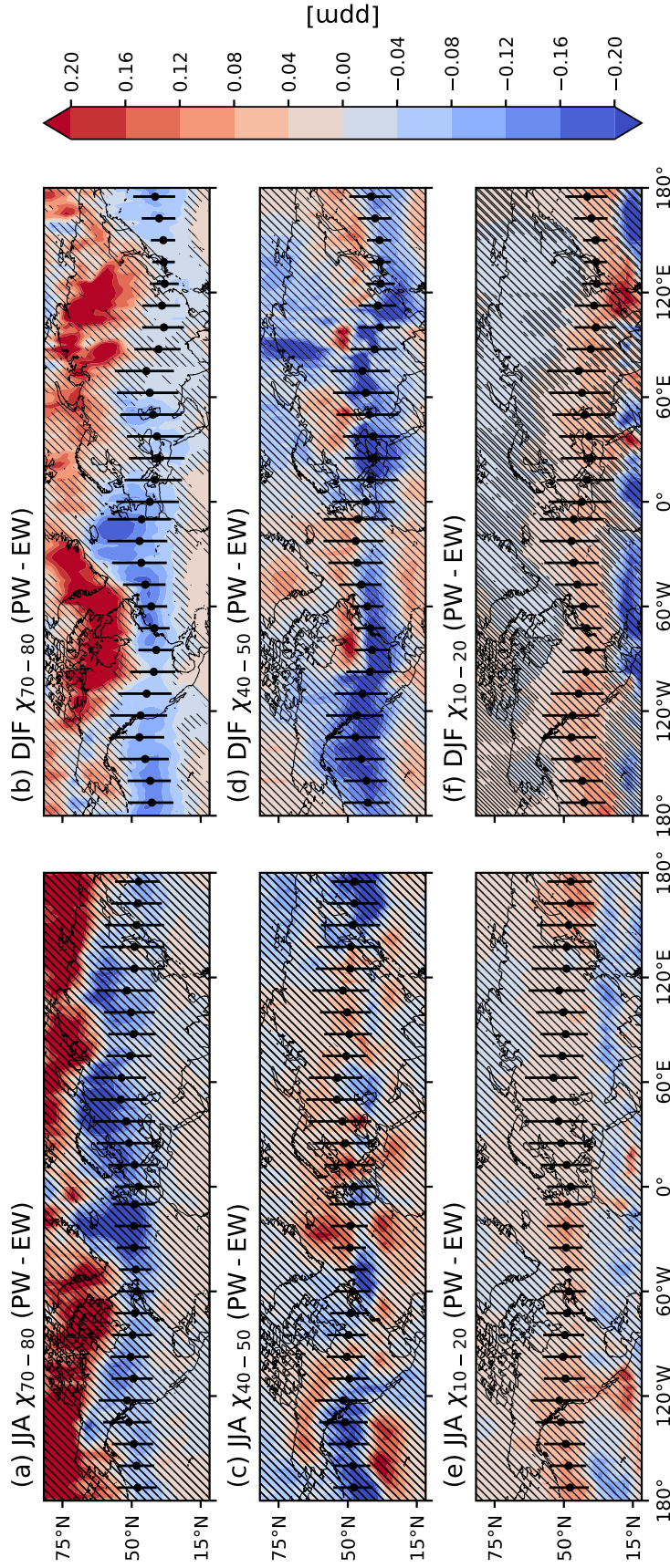


**Figure 2.** The difference in composites of JJA (a)  $\chi_{10-20}$ , (c)  $\chi_{40-50}$ , and (e)  $\chi_{70-80}$  for days with a PW versus EW jet stream. Hatching denotes tracer-jet correlations that are not statistically significant. Scatter points and vertical bars represent the mean position and variability of the jet stream in JJA, respectively. (b), (d), and (f) are the same as (a), (c), and (e) but for DJF.

acterized by  $\partial\chi/\partial\phi > 0$  in the mid-latitudes and decrease in the mid-latitudes when the jet is PW (Figure 2e-f).

Beyond the mid-latitudes and these three tracers, impact of source region on the tracer-jet relationships for all the GEOS-Chem tracers can be easily seen in the zonal mean (Figure 3a-b). The tracer-jet relationships all exhibit an oscillatory pattern, but tracers with source regions south of the range of the jet are positively correlated with the jet in the mid-latitudes and are flanked by negative correlations (although generally not significant) outside the mid-latitudes. Tracers with source regions north of the jet have a negative correlation with the jet in the mid-latitudes and a positive, but non-statistically significant, correlation outside the mid-latitudes (Figure 3a-b).

The variations in tracer mixing ratios related to the meridional oscillations of the jet are a sizable fraction of the overall daily tracer variability discussed earlier in this section. For example, the ratios of the jet-associated variations in  $\chi_{10-20}$ ,  $\chi_{40-50}$ , and  $\chi_{70-80}$  to the overall variability (standard deviation) zonally-averaged over the mid-latitudes ( $40^\circ < \phi < 60^\circ\text{N}$ ) are 58%, 35%, and 47%, respectively.

In a gross sense, the relationship between the jet stream and our tracers does not change in DJF compared to JJA, but further inspection indicates that there are nuanced differences in the relationships (Figure 2). For example, the change in mid-latitude mixing ratios of  $\chi_{40-50}$  due to the meridional movement of the jet is varied in sign and strength during JJA, while the DJF change is largely negative (Figure 3b-c).

We also evaluate how tracer lifetime impacts the tracer-jet relationships within GEOS-Chem by simulating  $\chi_{40-50}$  with loss rates ranging from 5 to 150 days (Section 2). The relationship of the jet with  $\chi_{40-50}$  for loss rates  $\geq 5 \text{ days}^{-1}$  are virtually identical in sign and significance to  $\chi_{40-50}$  with the 50 day $^{-1}$  loss rate discussed elsewhere in this study (not shown), although the precise magnitude of the variability associated with the jet changes with tracer lifetime. Thus, the jet is an important source of variability for surface-level trace species spanning a wide range of lifetimes.

### 3.2 Mechanisms

The analysis presented in Section 3.1 has shown that a large fraction of daily tracer variability is related to meridional movement of the jet but does not show the mechanism(s) involved or why the signs of the tracer-jet relationships varies. Kerr et al. (2020) suggested that the jet stream affects surface-level  $\text{O}_3$  by altering the near-surface meridional flow ( $V$ ). We test this hypothesis using our suite of tracers. We first examine the  $V$ -jet relationship and then how this impacts the tracers.

Figure 3c indicates that southerly flow increases in the mid-latitudes (around the latitudinal range of the jet stream) when the jet is PW during JJA and DJF; however, it does not show the magnitude. As is shown in Figure 4a-b,  $V$  increases over 5 m/s in parts of the mid-latitudes when the jet is PW. This stands in sharp contrast to time-averaged  $V$ , which is generally weak ( $-2 < V < 2 \text{ m/s}$ ) over the vast majority of the mid-latitudes. It is exceedingly rare for time-averaged  $V$  to have the same magnitude changes in  $V$  linked to the jet (contours in Figure 3a-b). Outside the mid-latitudes, the relationship between  $V$  and  $\phi_{jet}$  is largely non-significant and weak (Figures 3c, 4a-b).

The  $V$ -jet relationship is not zonally-symmetric (Figure 4a-b). For example, the JJA  $V$ -jet relationship is negative over the mid-latitude oceans on the windward shores of the continents but is positive over the mid-latitude continents and the leeward shores (Figure 4a).

In the zonal mean, the latitudes, or nodes, where  $r(\chi, \phi_{jet}) = 0$  are well-aligned with the latitudes where the jet stream and  $V$  are not correlated (Figure 3). The only node where  $r(V, \phi_{jet}) = 0$  does not coincide with  $r(\chi, \phi_{jet}) = 0$  occurs during DJF

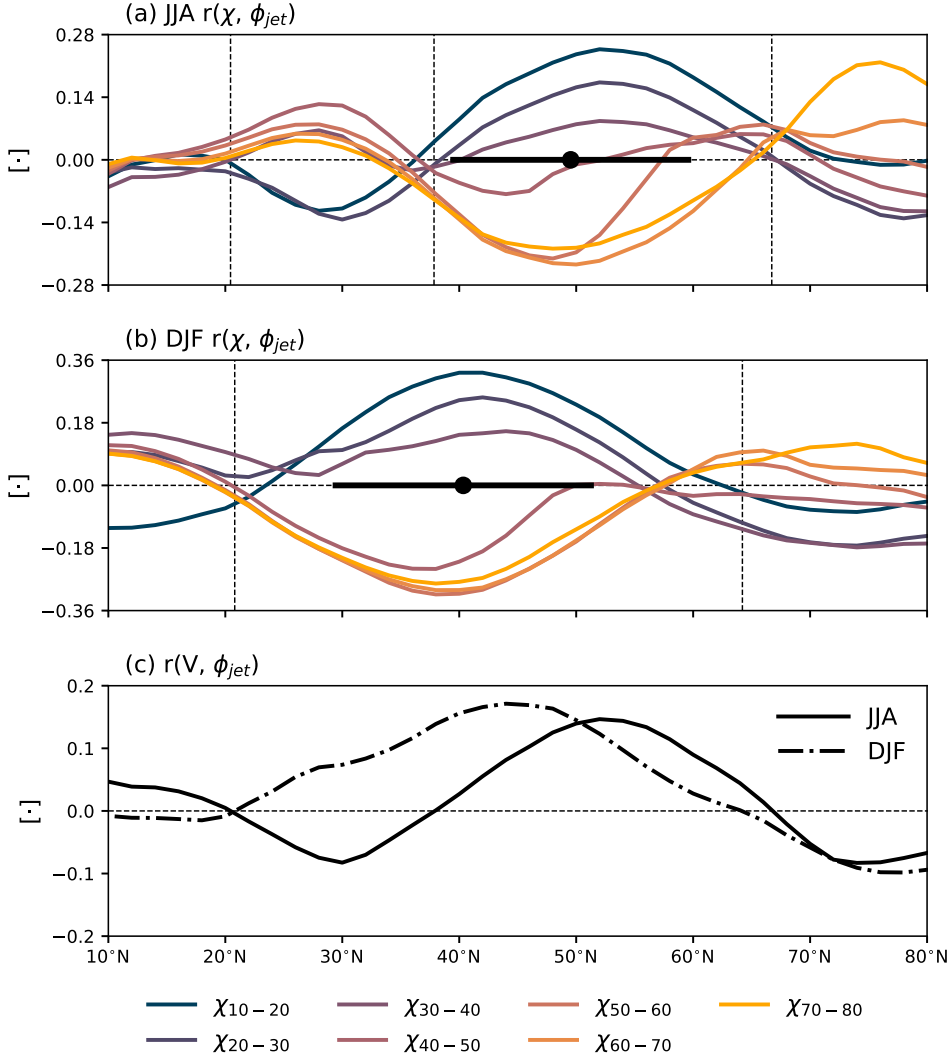


**Figure 3.** An illustration of how  $\phi_{jet}$  impacts near-surface  $V$  and tracers. (a) The JJA zonally-averaged correlation between  $\phi_{jet}$  and individual tracers (colors) and the mean position and variability of the jet stream (scatter point and horizontal bars). (b) same as (a) but for DJF. (c) Zonally-averaged  $r(V, \phi_{jet})$ . Dashed vertical lines in (a)-(b) denote the latitudes where  $r(V, \phi_{jet}) = 0$  for each season. Dashed horizontal lines separate positive from negative correlations.

237 north of the jet (Figure 3b). In this case, the latitude where  $r(V, \phi_{jet}) = 0$  lies north  
 238 of  $r(\chi, \phi_{jet}) = 0$  by  $\sim 5^\circ$ , and other processes could be important for the tracer-jet re-  
 239 lationships in this region and season. These results support Kerr et al. (2020) and pro-  
 240 vide strong evidence linking the tracer-jet relationships to (1) the source region of the  
 241 tracers and (2) the  $V$ -jet relationship (Figure 3).

242 The jet-induced change in  $V$  modifies meridional tracer advection (i.e.,  $-V \cdot \partial\chi/\partial\phi$ ).  
 243 Thus, the impact of a given change in  $V$  is expected to depend on the local tracer gra-  
 244 dients. If  $\partial\chi/\partial\phi$  is weak, then smaller tracer changes are expected compared with lo-  
 245 cations with stronger  $\partial\chi/\partial\phi$ . It also follows that the same change in  $V$  operating over

246  $\partial\chi/\partial\phi < 0$  versus  $\partial\chi/\partial\phi > 0$  would result in changes of tracer mixing ratios with dif-  
 247 ferent signs. Given this, we postulate that the expected sign of the tracer-jet relation-  
 248 ships ( $E[r(\chi, \phi_{jet})]$ ) shown in Figures 2-3 can be approximated by:

$$249 \quad E[r(\chi, \phi_{jet})] \sim -r(V, \phi_{jet}) \cdot \frac{\partial\chi}{\partial\phi}. \quad (1)$$

250 In practice, this balance implies that the anomalous southerly flow in the mid-latitudes  
 251 that accompanies a PW-shifted jet ( $r(V, \phi_{jet}) > 0$ ) will advect higher tracer mixing ra-  
 252 tios from lower latitudes if  $\partial\chi/\partial\phi < 0$ , yielding a positive expected tracer-jet relation-  
 253 ship (i.e.,  $E[r(\chi, \phi_{jet})] > 0$ ).

254 The simple balance in Equation 1 robustly captures the large-scale differences in  
 255 the sign of the relationship between the jet and all tracers. We illustrate this for  $\chi_{40-50}$   
 256 in Figure 4c-d. The application of Equation 1 can explain the widespread negative  $\chi_{40-50}$ -  
 257 jet relationship in mid-latitudes during boreal winter (DJF) (Figure 4d) but also the dif-  
 258 ferences in sign on much smaller spatial scales during JJA (Figure 4c). Moreover, we note  
 259 that Equation 1 captures the land-ocean contrasts present in the JJA  $\chi_{40-50}$ -jet rela-  
 260 tionship (Figure 4c).

261 The application of Equation 1 does not capture the sign of the  $\chi_{40-50}$ -jet relation-  
 262 ship in the vicinity of the Atlantic and Pacific storm tracks (Figure 4c-d), and this is the  
 263 case for other tracers as well (not shown). Since our tracer mixing ratios are roughly zonally-  
 264 symmetric (Figure 1b-d), the effect of changes in the zonal wind are negligible to first  
 265 order. However, the jet stream exerts an influence on near-surface  $U$  (Woollings et al.,  
 266 2010), especially near the exit region of the these storm tracks. To account for this, fu-  
 267 ture studies could consider the impact of both the  $V$ -jet and  $U$ -jet relationships.

268 The zonal variations in the tracer-jet relationships shown above could stem from  
 269 zonal variations in the response of  $V$  to the movement of the jet *or* zonal variations in  
 270 the tracer gradients. To explore this, we have isolated the terms in Equation 1 by sep-  
 271 arately fixing each to its zonal mean value and thereafter recalculating  $E[r(\chi, \phi_{jet})]$  to  
 272 gauge which exerts a stronger influence on the tracer-jet relationships (not shown). Re-  
 273 calculating Equation 1 with  $\partial\chi/\partial\phi$  fixed to its zonal mean value and  $r(V, \phi_{jet})$  varying  
 274 as in Figure 4a-b yields expected tracer-jet relationships with zonal variations that re-  
 275 semble the relationships shown in Figure 4c-d. This sensitivity test together with the anal-  
 276 ysis performed in Figure 4c-d confirm spatiotemporal variations in the  $V$ -jet relation-  
 277 ship are the most important factor in explaining the tracer-jet coupling, followed by the  
 278 latitudinal tracer gradient.

279 The importance of the jet stream and meridional flow on daily tracer variability  
 280 is not restricted to only near-surface mixing ratios but holds for tropospheric column abun-  
 281 dances. To support this, we repeat the analyses shown in Figures 3-4 but with  $V$  and  
 282 mass-weighted tracer mixing ratios from 1000–200 hPa (Figures S1-S2) to show that  
 283 the  $V$ -jet relationship not only explains variations in near-surface mixing ratios but also  
 284 in tropospheric column tracer mixing ratios.

## 285 4 Conclusions

286 This study demonstrates that the daily variability of the position of the jet stream  
 287 has a strong influence on near-surface tracer mixing ratios within the seasonally-dependent  
 288 latitude range of the jet but a weak relationship outside this range. The sign of the jet-  
 289 tracer relationship varies with the latitude of tracer source and the resulting meridional  
 290 tracer gradients (Figures 2, 3a-b). Tracers with a negative gradient within the latitudi-  
 291 nal range of the jet have positive tracer-jet relationships in the mid-latitudes, while the  
 292 opposite is true for tracers with positive gradients within the jet's range. Tracers whose

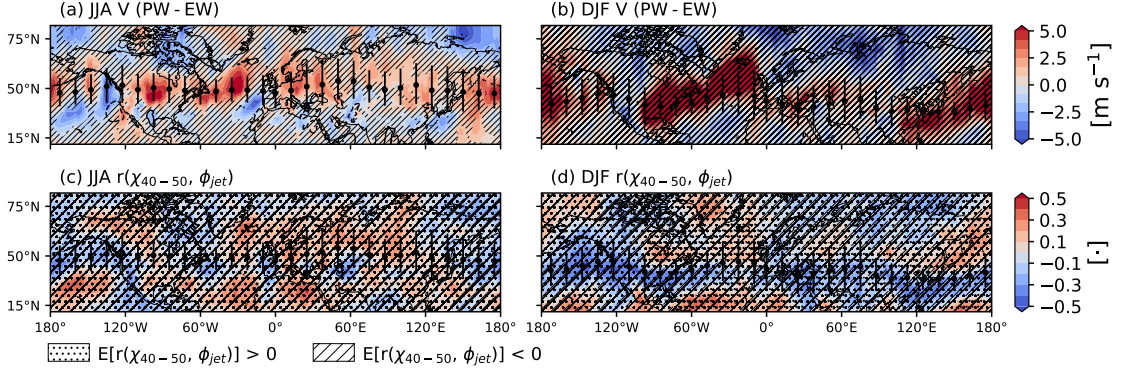


**Figure 4.** (a-b) Differences in composites of  $V$  for days with a PW versus EW jet stream (colours). Time-averaged  $V$  is illustrated for 5 m/s (solid black contour) and  $-5$  m/s (dashed black contour). Hatching denotes statistically non-significant  $V$ -jet correlations. (c-d) The correlation coefficient calculated between  $\chi_{40-50}$  and  $\phi_{jet}$  (colours). As denoted in the legend beneath (c), stippling and hatching show the expected sign of the correlation,  $E[r(\chi_{40-50}, \phi_{jet})]$ , determined using Equation 1. Scatter points and vertical bars in all subplots represent the mean position of and variability of the jet stream, respectively.

293 source regions lie within the latitudinal range of the jet have a zonally-varying meridional  
 294 gradient and subsequently a zonally-asymmetric relationship with the jet in the mid-  
 295 latitudes. Strong jet-tracer relationships are found for both JJA and DJF, but the lat-  
 296 itudes with the strongest relationships vary with the seasonal movement of the mean jet  
 297 latitude.

298 We show that the mechanism that connects the upper-level jet to variability near-  
 299 surface composition is changes in near-surface meridional flow that result from the merid-  
 300 ional movement of the jet stream. This mechanism explains (1) the variation in sign of  
 301 the jet-tracer relationship with tracer meridional gradients, (2) the land-ocean differences  
 302 in the jet-tracer relationship for tracers with mid-latitude sources, and (3) seasonal dif-  
 303 ferences in the jet-tracer relationship. Furthermore, this mechanism explains both the  
 304 latitudinal and land-ocean differences in the JJA jet-O<sub>3</sub> relationship reported in Kerr  
 305 et al. (2020) and also helps explain seasonality in the jet-O<sub>3</sub> relationship. Although not  
 306 shown in Kerr et al. (2020), the sign of the jet-O<sub>3</sub> relationship over North America and  
 307 Eurasia changes from positive during JJA to negative in DJF, which is broadly consist-  
 308 ent with  $\chi_{40-50}$  (Figures 2c-d, 4c-d).

309 The jet-tracer relationships found in our simulations hold for a wide range of tracer  
 310 lifetimes (5 to 150 days) and for mass-weighted tropospheric column mixing ratios. Thus,  
 311 our results may be useful for interpreting variations in a host of species, including the  
 312 total column measurements commonplace among satellite products. Contemporaneous  
 313 studies have found that variations in meteorology can explain a substantial portion of  
 314 total column observations of greenhouse gases, comparable to the impact of regional vari-  
 315 ations in surface fluxes (e.g., Keppel-Aleks et al., 2011). Differentiating whether patterns  
 316 in satellite observations are due to transport versus variations in surface fluxes may help  
 317 explain differences in trace gas distributions due to large-scale transport. Future stud-  
 318 ies should test this possibility.

319 Our study has documented a major driver of near-surface composition variability  
 320 (i.e., transport associated with the jet stream) and linked this driver with the location

321 of emissions. This finding is relevant for understanding possible future changes of tracer  
 322 variability, as models predict that the jet stream will migrate north (e.g., Barnes & Polvani,  
 323 2013), which will modify the poleward transport of air pollution and greenhouse gases  
 324 via its regulation of the near-surface meridional flow. In addition, there is a redistribu-  
 325 tion of anthropogenic emissions from the mid-latitudes (developed nations) to low lat-  
 326 itudes (developing nations) (Zhang et al., 2016), which may change meridional tracer gra-  
 327 dients and the daily variations connected to the jet. Further research is needed to quan-  
 328 tify the impact of these possible changes in the jet and emissions.

### 329 Acknowledgments

330 This work is supported by NASA’s Atmospheric Composition Modeling and Analysis  
 331 Program (Grant No. NNX17AI31G) and NSF’s Integrative Graduate Education and Re-  
 332 search Traineeship Program (Grant No. 1069213). GEOS-Chem simulations were run  
 333 on the Maryland Advanced Research Computing Center (MARCC). NASA’s Global Mod-  
 334 eling and Assimilation Office and Goddard Earth Sciences Data and Information Ser-  
 335 vices Center (GES DISC) provided and disseminated the MERRA-2 data used in this  
 336 study, specifically the `inst3_3d_asm_Np` collection (Global Modeling and Assimilation Of-  
 337 fice (GMAO), 2015).

### 338 References

- 339 Barnes, E. A., & Fiore, A. M. (2013). Surface ozone variability and the jet posi-  
 340 tion: Implications for projecting future air quality. *Geophys. Res. Lett.*, *40*(11),  
 341 2839–2844. doi: 10.1002/grl.50411
- 342 Barnes, E. A., & Polvani, L. (2013). Response of the midlatitude jets, and of their  
 343 variability, to increased greenhouse gases in the CMIP5 models. *J. Clim.*,  
 344 *26*(18), 7117–7135. doi: 10.1175/JCLI-D-12-00536.1
- 345 Bey, I., Jacob, D. J., Yantosca, R. M., Logan, J. A., Field, B. D., Fiore, A. M., et al.  
 346 (2001). Global modeling of tropospheric chemistry with assimilated meteorol-  
 347 ogy: Model description and evaluation. *J. Geophys. Res. Atmos.*, *106*(D19),  
 348 23073–23095. doi: 10.1029/2001jd000807
- 349 Bosilovich, M., Akella, S., Coy, L., Cullather, R., Draper, C., Gelaro, R., et al.  
 350 (2015). *MERRA-2: Initial evaluation of the climate, NASA/TM-2015-104606*  
 351 (Vol. 43).
- 352 Cooper, O. R., Parrish, D. D., Ziemke, J., Balashov, N. V., Cupeiro, M., Gal-  
 353 bally, I. E., et al. (2014). Global distribution and trends of tropospheric  
 354 ozone: An observation-based review. *Elem. Sci. Anth.*, *2*, 000029. doi:  
 355 10.12952/journal.elementa.000029
- 356 Dawson, J. P., Bloomer, B. J., Winner, D. A., & Weaver, C. P. (2014). Under-  
 357 standing the meteorological drivers of U.S. particulate matter concentra-  
 358 tions in a changing climate. *Bull. Amer. Meteor. Soc.*, *95*(4), 521–532. doi:  
 359 10.1175/bams-d-12-00181.1
- 360 Gelaro, R., McCarty, W., Suárez, M. J., Todling, R., Molod, A., Takacs, L., et  
 361 al. (2017). The Modern-Era Retrospective Analysis for Research and  
 362 Applications, Version 2 (MERRA-2). *J. Clim.*, *30*(14), 5419–5454. doi:  
 363 10.1175/JCLI-D-16-0758.1
- 364 Global Modeling and Assimilation Office (GMAO). (2015).  
 365 *MERRA-2 inst3\_3d\_asm\_Np:3d,3-Hourly,Instantaneous,Pressure-*  
 366 *Level,Assimilation,Assimilated Meteorological Fields V5.12.4*. Greenbelt, MD,  
 367 USA. (Last accessed: 25 September 2019) doi: 10.5067/QBZ6MG944HW0
- 368 Guha, T., Tiwari, Y. K., Valsala, V., Lin, X., Ramonet, M., Mahajan, A., ...  
 369 Kumar, K. R. (2018). What controls the atmospheric methane sea-  
 370 sonal variability over India? *Atmos. Environ.*, *175*, 83–91. doi: 10.1016/  
 371 j.atmosenv.2017.11.042

- 372 Jacob, D. J., Logan, J. A., Gardner, G. M., Yevich, R. M., Spivakovsky, C. M.,  
 373 Wofsy, S. C., et al. (1993). Factors regulating ozone over the United States  
 374 and its export to the global atmosphere. *J. Geophys. Res.*, *98*(D8), 14817. doi:  
 375 10.1029/98jd01224
- 376 Keppel-Aleks, G., Wennberg, P. O., & Schneider, T. (2011). Sources of variations in  
 377 total column carbon dioxide. *Atmos. Chem. Phys.*, *11*(8), 3581–3593. doi: 10  
 378 .5194/acp-11-3581-2011
- 379 Kerr, G. H., Waugh, D. W., Steenrod, S. D., Strode, S. A., & Strahan, S. E. (2020).  
 380 Surface ozone-meteorology relationships: Spatial variations and the role of  
 381 the jet stream. *Submitted to J. Geophys. Res. Atmos.*. Retrieved from  
 382 <https://www.essoar.org/doi/10.1002/essoar.10502500.2>
- 383 Kerr, G. H., Waugh, D. W., Strode, S. A., Steenrod, S. D., Oman, L. D., & Strahan,  
 384 S. E. (2019). Disentangling the drivers of the summertime ozone-temperature  
 385 relationship over the United States. *J. Geophys. Res.*, *124*(19), 10503–10524.  
 386 doi: 10.1029/2019jd030572
- 387 Law, K. S., & Stohl, A. (2007). Arctic air pollution: Origins and impacts. *Science*,  
 388 *315*(5818), 1537–1540. doi: 10.1126/science.1137695
- 389 Liu, H., Jacob, D. J., Bey, I., & Yantosca, R. M. (2001). Constraints from  $^{210}\text{Pb}$   
 390 and  $^7\text{Be}$  on wet deposition and transport in a global three-dimensional chemi-  
 391 cal tracer model driven by assimilated meteorological fields. *J. Geophys. Res.*  
 392 *Atmos.*, *106*(D11), 12109–12128. doi: 10.1029/2000jd900839
- 393 McCarty, W., Coy, L., Gelaro, R., Huang, A., Merkova, D., Smith, E. B., et al.  
 394 (2016). *MERRA-2 input observations: Summary and assessment* (Techni-  
 395 cal Report Series on Global Modeling and Data Assimilation, Volume 46).  
 396 Greenbelt, MD, USA: National Aeronautics and Space Administration.
- 397 Miller, S. M., Hayek, M. N., Andrews, A. E., Fung, I., & Liu, J. (2015). Biases in at-  
 398 mospheric  $\text{CO}_2$  estimates from correlated meteorology modeling errors. *Atmos.*  
 399 *Chem. Phys.*, *15*(5), 2903–2914. doi: 10.5194/acp-15-2903-2015
- 400 Miller, S. M., Wofsy, S. C., Michalak, A. M., Kort, E. A., Andrews, A. E., Bi-  
 401 raud, S. C., et al. (2013). Anthropogenic emissions of methane in the  
 402 United States. *Proc. Natl. Acad. Sci. U.S.A.*, *110*(50), 20018–20022. doi:  
 403 10.1073/pnas.1314392110
- 404 Mudelsee, M. (2003). Estimating Pearson’s correlation coefficient with bootstrap  
 405 confidence interval from serially dependent time series. *Math. Geol.*, *35*(6),  
 406 651–665. doi: 10.1023/b:matg.0000002982.52104.02
- 407 Orbe, C., Waugh, D. W., Newman, P. A., & Steenrod, S. (2016). The transit-time  
 408 distribution from the Northern Hemisphere midlatitude surface. *J. Atmos.*  
 409 *Sci.*, *73*(10), 3785–3802. doi: 10.1175/jas-d-15-0289.1
- 410 Orbe, C., Waugh, D. W., Yang, H., Lamarque, J.-F., Tilmes, S., & Kinnison, D. E.  
 411 (2017). Tropospheric transport differences between models using the same  
 412 large-scale meteorological fields. *Geophys. Res. Lett.*, *44*(2), 1068–1078. doi:  
 413 10.1002/2016gl071339
- 414 Orbe, C., Yang, H., Waugh, D. W., Zeng, G., Morgenstern, O., Kinnison, D. E., et  
 415 al. (2018). Large-scale tropospheric transport in the Chemistry-Climate Model  
 416 Initiative (CCMI) simulations. *Atmos. Chem. Phys.*, *18*(10), 7217–7235. doi:  
 417 10.5194/acp-18-7217-2018
- 418 Ordóñez, C., Barriopedro, D., & García-Herrera, R. (2019). Role of the position of  
 419 the North Atlantic jet in the variability and odds of extreme  $\text{PM}_{10}$  in Europe.  
 420 *Atmos. Environ.*, *210*, 35–46. doi: 10.1016/j.atmosenv.2019.04.045
- 421 Pal, S., Davis, K. J., Lauvaux, T., Browell, E. V., Gaudet, B. J., et al. (2020).  
 422 Observations of greenhouse gas changes across summer frontal boundaries  
 423 in the Eastern United States. *J. Geophys. Res. Atmos.*, *125*(5). doi:  
 424 10.1029/2019jd030526
- 425 Porter, W. C., & Heald, C. L. (2019). The mechanisms and meteorological drivers of  
 426 the ozone-temperature relationship. *Atmos. Chem. Phys.*, 13367–13381. doi: 10

- 427 .5194/acp-2019-140  
428 Randazzo, N. A., Michalak, A. M., & Desai, A. R. (2020). Synoptic meteorology  
429 explains temperate forest carbon uptake. *J. Geophys. Res. Biogeosci.*, *125*(2).  
430 doi: 10.1029/2019jg005476
- 431 Shen, L., Mickley, L. J., & Tai, A. P. K. (2015). Influence of synoptic patterns on  
432 surface ozone variability over the eastern United States from 1980 to 2012. *At-*  
433 *mos. Chem. Phys.*, *15*(19), 10925–10938. doi: 10.5194/acp-15-10925-2015
- 434 Shindell, D. T., Chin, M., Dentener, F., Doherty, R. M., Faluvegi, G., Fiore, A. M.,  
435 et al. (2008). A multi-model assessment of pollution transport to the Arctic.  
436 *Atmos. Chem. Phys.*, *8*(17), 5353–5372. doi: 10.5194/acp-8-5353-2008
- 437 The International GEOS-Chem User Community. (2018, October 10).  
438 *geoschem/geos-chem: Geos-chem 12.0.2 release (Version 12.0.2)*. Zenodo.  
439 Retrieved from <http://doi.org/10.5281/zenodo.1455215>
- 440 Torres, A. D., Keppel-Aleks, G., Doney, S. C., Fendrock, M., Luis, K., Mazière,  
441 M. D., et al. (2019). A geostatistical framework for quantifying the imprint of  
442 mesoscale atmospheric transport on satellite trace gas retrievals. *J. Geophys.*  
443 *Res. Atmos.*, *124*(17-18), 9773–9795. doi: 10.1029/2018jd029933
- 444 Wilks, D. S. (1997). Resampling hypothesis tests for autocorrelated fields. *J. Clim.*,  
445 *10*(1), 65–82. doi: 10.1175/1520-0442(1997)010<0065:rhtfaf>2.0.co;2
- 446 Wilks, D. S. (2011). *Statistical methods in the atmospheric sciences*. Amsterdam;  
447 Boston: Elsevier Academic Press.
- 448 Woollings, T., Hannachi, A., & Hoskins, B. (2010). Variability of the North Atlantic  
449 eddy-driven jet stream. *Q. J. R. Meteorol. Soc.*, *136*(649), 856–868. doi: 10  
450 .1002/qj.625
- 451 Yang, H., Waugh, D. W., Orbe, C., Zeng, G., Morgenstern, O., Kinnison, D. E., et  
452 al. (2019). Large-scale transport into the Arctic: The roles of the midlati-  
453 tude jet and the Hadley cell. *Atmos. Chem. Phys.*, *19*(8), 5511–5528. doi:  
454 10.5194/acp-19-5511-2019
- 455 Yu, K., Keller, C. A., Jacob, D. J., Molod, A. M., Eastham, S. D., & Long, M. S.  
456 (2018). Errors and improvements in the use of archived meteorological data  
457 for chemical transport modeling: An analysis using GEOS-Chem v11-01  
458 driven by GEOS-5 meteorology. *Geosci. Model Dev.*, *11*(1), 305–319. doi:  
459 10.5194/gmd-11-305-2018
- 460 Zhang, Y., Cooper, O. R., Gaudel, A., Thompson, A. M., Nédélec, P., Ogino, S.-Y.,  
461 & West, J. J. (2016). Tropospheric ozone change from 1980 to 2010 dominated  
462 by equatorward redistribution of emissions. *Nat. Geosci.*, *9*(12), 875–879. doi:  
463 10.1038/ngeo2827
- 464 Zhuang, J., Dussin, R., Jüling, A., & Rasp, S. (2020). *Jiaweizhuang/xesmf: v0.3.0*  
465 *adding esmf.locstream capabilities*. Zenodo. Retrieved from [https://zenodo](https://zenodo.org/record/1134365)  
466 [.org/record/1134365](https://zenodo.org/record/1134365) doi: 10.5281/ZENODO.1134365